Siberian Arctic black carbon: gas flaring and wildfire impact

Olga B. Popovicheva[1], Nikolaos Evangeliou[2,*], Vasilii O. Kobelev[3], Marina A. Chichaeva[4], Konstantinos Eleftheriadis[5], Asta Gregorič[6,7], Nikolay S. Kasimov[4]

[1] SINP, Lomonosov Moscow State University, 119991 Moscow, Russia
[2] NILU - Norwegian Institute for Air Research, 2007 Kjeller, Norway
[3]Moscow Department of Russian Geographical Society, Moscow, Russia
[4]Geographical Department, Lomonosov Moscow State University, 119991 Moscow, Russia
[5]ERL, Institute of Nuclear and Radiological Science & Technology, Energy & Safety, N.C.S.R. Demokritos, 15341 Attiki, Greece
[6]Aerosol d.o.o., SI-1000, Ljubljana, Slovenia
[7]Center for Atmospheric Research, University of Nova Gorica, SI-5270, Ajdovščina, Slovenia

* Corresponding authors: N. Evangeliou (Nikolaos.Evangeliou@nilu.no)

Abstract

As explained in the latest Arctic Monitoring and Assessment Programme (AMAP) report released in early 2021, the Arctic has warmed three times more quickly than the planet as a whole, and faster than previously thought. The Siberian Arctic is of great interest largely because observations are sparse or largely lacking. A research aerosol station has been developed on the Bely Island (Kara Sea) in Western Siberia. Measurements of equivalent black carbon (EBC) concentrations were carried out at the "Island Bely" station continuously from August 2019 to November 2020. The source origin of the measured EBC, and the main contributing sources were assessed using atmospheric transport modelling coupled with the most updated emission inventories for anthropogenic and biomass burning sources of BC.

The obtained climatology for BC during the period of measurements showed an apparent seasonal variation with the highest concentrations between December and April (60±92 ng/m3) and the lowest between June and September (18±72 ng/m3), typical of the Arctic Haze seasonality reported elsewhere. When air masses arrived at the station through the biggest oil and gas extraction regions of Kazakhstan, Volga-Ural, Komi, Nenets and Western Siberia, BC contribution from gas flaring dominated over domestic, industrial, and traffic sectors, ranging from 47 to 68%, with a maximum contribution in January. When air was transported from Europe during the cold season, emissions from transportation were more important. Accordingly, shipping emissions increased due to the touristic cruise activities and the ice retreat in summertime. Biomass burning (BB) played the biggest role between April and October, contributing 81% at maximum in July. Long-range transport of BB aerosols appeared to induce large variability to the Absorption Ångström Exponent (AAE) with values ranging >1.0 (excluding outliers). As regards to the continental contribution to surface BC at the "Island Bely" station, Russian emissions dominated during the whole year, while European and Asian ones contributed up to 20% in the cold period. Quantification of several pollution episodes showed an increasing trend in surface concentrations and frequency during the cold period, as the station is directly in the Siberian gateway of the highest anthropogenic pollution sources to the Russian Arctic.

Deleted: ,

Deleted: ,

Deleted: BC

Deleted: comprising

Deleted: became

Deleted: June

Deleted: from 1.2 to

Deleted:

Deleted: 4

Deleted: emissions

1 Introduction

Global carbon pollution is annually produced by burning of fossil fuel and biomass. Combustion emissions are increasingly recognized as an important source of chemically active aerosols. Black carbon (BC) originates from the incomplete combustion of fossil fuels and biomass burning; it is a short-lived climate forcer and absorbs incoming solar radiation and, therefore, is of high significance for the Arctic climate (Wang et al., 2011). The combined total effects of BC and sulfates cause an Arctic surface warming of +0.29°K explaining approximately 20% of the observed Arctic warming since the early 1980s (Ren et al., 2020). BC resides in the lowest atmospheric layer, affects aerosol-cloud interactions (Yun et al., 2013) and has a cloud and sea-ice feedback when deposited (Flanner, 2013), thus accelerating melting (Quinn et al., 2008).

Long-range transport to the Arctic carries, among other aerosol constituents, many tracers of anthropogenic and wildfire origin (Chang et al., 2011). (Winiger et al., 2016) showed that BC in Arctic Scandinavia is predominantly linked to emissions in Europe. Over the whole Arctic region (north of 66°N), Russia contributes 62% to surface BC (Zhu et al., 2020). Industrial and residential sources are responsible for the highest measured BC concentrations at the Tiksi station (Siberian Arctic) (Popovicheva et al., 2019b). (Stathopoulos et al., 2021) have demonstrated that the long term impact of light absorbing carbon in the high Arctic is three times higher in the cold period of the year compared to the warm period. There, fossil sources mostly prevail during winter-spring season, while biomass burning sources dominate during low BC concentration periods in summer (Winiger et al., 2017). Although BC dominates light absorption by atmospheric aerosols, other carbonaceous aerosol species (brown carbon, BrC) represent an important fraction of light absorption in the UV and near-UV spectrum, thus having an important role in the assessment of radiative forcing in the Arctic climate. Spectral dependence of the light absorption is generally described by the Absorption Ångström Exponent (AAE), which is typically used to differentiate between aerosol types (BC, BrC) and sources of BC (Sandradewi et al., 2008; Helin et al., 2021; Zotter et al., 2017).

Quantification of the particulate Arctic pollution is a serious problem worldwide; reliable source emission inventories are challenged, and regional contributions of BC sources in the Arctic are still inconclusive (Zhu et al., 2020). Global anthropogenic emission dataset ECLIPSEv6 (Evaluating the Climate and Air Quality Impacts of Short-lived Pollutants) using the GAINS model (Klimont et al., 2017) includes all major economic sectors, such as energy and industrial production, transport, residential combustion, agriculture, and waste, distinguishing between sector-fuel-technology, fuels, and emission control options. The model predictions for European

Deleted:
Deleted: activities
Deleted: s
Deleted: absorption
Deleted: exponent
Deleted: different
Deleted: for the source apportionment
Deleted: the

gateway to the Arctic were greatly improved, when the emission inventory from anthropogenic sources was updated by estimates of European BC emissions (Winiger et al., 2016).

Due to large size and continuous production, gas flaring of oil industry is one of the highest BC emission sources (Ismail and Umukoro, 2012) with a strong environmental and climatic impact for the Arctic (Cho et al., 2019). Flaring in ECLIPSEv6 dominates BC emissions in the Arctic; models have found that flaring contributes 42% to the annual mean BC surface concentrations in the Arctic (Stohl et al., 2013). However, because flares are difficult to measure, their particulate emissions and physicochemical properties are still underestimated (Conrad and Johnson, 2017; Popovicheva et al., 2019a). Currently, models are struggling to reproduce BC concentrations largely due to emission-related uncertainties in the Arctic region (Schacht et al., 2019). The observed annual mean contribution of fossil fuel combustion to the Arctic concentrations agrees within a factor of two (Qi and Wang, 2019).

High latitude flaring emissions mainly originate from the North Sea, Norwegian Sea, the northeastern part of European Russia (Komi Republic) and Western Siberia. The largest oil and gas producing regions of northwestern Siberia are located along the main low-level pathway of air masses entering the Arctic and thus have a disproportionally large contribution to the Arctic lower troposphere (Stohl, 2006). (Eleftheriadis et al., 2009) and (Tunved et al., 2013) identified these regions as a key source for the highest measured BC concentrations and sub-micrometer aerosol mass concentrations, respectively, at the Zeppelin station. The impact of BC long-range transport from northwestern Siberia was also observed at the Ice Base Cape Baranova station located on Severnaya Zemlya archipelago (Eastern Siberia) (Manousakas et al., 2020). Accordingly, possible gas flaring impact was observed at the Tiksi station (northeastern Siberia), despite the large distance of the station from the largest oil and gas producing regions (Winiger et al., 2017). To better understand and quantify the contribution of gas flaring to the Arctic environment, targeted aerosol and atmospheric composition measurements at the closest distance from the flaring facilities are needed. The present operating Eurasian Arctic stations are all too far away to allow assessing how air masses are affected by gas flares or what the contribution from different source categories is (Stohl et al., 2013). Simulations combined with observations of BC at the proximity of the source regions (e.g., the plumes from gas flaring regions over the Kara Sea) provide a better constraint (Popovicheva et al., 2017). In addition, measurements of BC coupled by conditional probability simulations performed inside the oil and gas producing region of the northwestern Siberia have successfully distinguished between multiple industrial and urban sources (Popovicheva et al., 2020).

Deleted: of

Deleted: amended

Deleted: inventories

Deleted: The h

Deleted: mainly

Deleted: consistency

Deleted: at the Polar circle

Deleted: separated

Deleted: the

Recent efforts have sought to develop a new Russian BC emission inventory (BCRUS) for the Siberian Arctic, based on activity data from local information, improved spatial distribution of BC emissions and updated emission factors for oil and gas fields in northwestern Siberia (Huang et al., 2015). According to this, it was found that BC emissions from gas flaring account for 36% of the total anthropogenic BC emissions over Russia. Residential BC emissions, transportation, industry, and power plants contribute 25%, 20%, 13%, and 5.4%, respectively. The emissions from gas flaring in BCRUS show a discrepancy of more than 40% higher than ECLIPSEv5. Using BCRUS, modelled surface BC at Zeppelin, Barrow, and Alert stations were basically improved (Huang et al., 2015). The contribution of anthropogenic emissions in Russia to the annual total Arctic surface BC were calculated to be 56%, with gas flaring from the Yamalo-Nenets Autonomous Okrug (YNAO), Khanty-Mansiysk Autonomous Okrug (KMAO), and Komi Republic to be the main source (31% of Arctic surface BC) (Zhu et al., 2020). However, due to the absence of BC inventories for industrial emissions and a denser observational network in the western Siberian High Arctic, the spatial distribution of BC sources is still associated with large uncertainties.

Agricultural fires in East Europe and North America are a major source of biomass burning in the Eurasian Arctic (Treffeisen et al., 2007; Stohl et al., 2007; Stohl et al., 2006). Springtime fires in Siberia can double the North American Arctic background (Warneke et al., 2010). Long-term airborne observations of BC in Northern Siberia have revealed a strong impact from forest fires in summer (Kozlov et al., 2016; Paris et al., 2009). Particulate BrC emitted by intensive wildfires has been measured in plumes transported for over two days (Forrister et al., 2015). In summer 2019, wildfire activity in Central and Eastern Siberia occurred along the trans-Arctic transport pathway of Siberian biomass burning emissions resulting in enhanced aerosol lamina observed in Western Canada (Johnson et al., 2021).

In 2019, a new aerosol station was developed by Moscow State University on the Bely Island located in the Kara Sea (Western Siberian Arctic) (https://peexhq.home.blog/2019/12/11/new-research-aerosol-stations-in-the-russian-arctic), (Figure 1). The region was chosen because it is close to the air pathway of large-scale emission plumes from populated industrial regions of Eurasia and Siberian wildfires to the Arctic. We present here the ground-based continuous BC (equivalent BC, EBC) measurements from August 2019 until November 2020 at the "Island Bely" station for the first time. The Arctic annual trends of BC are assessed, while the geospatial source origin of the air arriving at the station is identified using a Lagrangian particle dispersion model. Furthermore, the anthropogenic and biomass burning contributions to the modelled surface concentrations of BC are evaluated against measured BC concentrations at the station.

Deleted: It
Deleted: the
Deleted: sector
Deleted: stations
Deleted: mostly
Deleted: represent
Deleted: being
Deleted: an official
Deleted: y
Deleted: of
Deleted: high
Deleted: e
Deleted: ern
Deleted: of
Deleted: brown carbon (
Deleted:)
Deleted: has been reported to be
Deleted: e
Deleted: and
Deleted: during
Deleted: western
Deleted: established
Formatted: Font: Not Bold
Formatted: Font: Not Bold, Not Italic, Check spelling and grammar
Deleted: Figure 1
Deleted: in
Deleted: Bely

Characterization of the pollution events in cold and warm periods separates the impact of gas flaring versus biomass burning. In addition, the spectrally resolved absorption measurements provide an opportunity for the characterization of BC sources. The present study assesses long range transport of BC to the Western Siberian Arctic from the main large-scale emission regions of the Eurasian continent using Lagrangian modelling coupled with continuous observations.

Deleted: distinguishes
Deleted: higher
Deleted: The
Deleted: attempts to
Deleted: the extent of
Deleted: ed plumes
Deleted: s from
Deleted: is attributed to BC emitted in the Western Siberian Arctic, by means of

2 Experimental

2.1 Aerosol station "Island Bely".

Western Siberia is the world's largest gas flaring region with a leading oil and gas production industry (**Figure 1**). YNAO is located north of the West Siberian Plain and covers a vast area of 769 thousand km^2. More than 94% of the region's economy is associated with industrial applications related to the extraction of fuels, their processing, and transportation. Specifically, YNAO has the largest reserves of Russia's natural gas and oil; YNAO emissions of BC are the largest in the Russian territory (Vinogradova, 2015). The relative contributions from gas flaring to annual mean BC surface concentrations from all emission sources (surface transportation, industry, residential, biomass burning) exceed 70% (Stohl et al., 2013).

Deleted: Figure 1
Deleted: 's
Deleted: BC
Deleted: approach
Deleted: a
Deleted: maximum through

The Bely Island is located in the Kara Sea, north of the YNAO (**Figure 1**). For the purpose of atmospheric composition observations and sampling at the "Island Bely" station, the aerosol pavilion has been built approximately half a km to the southeast of the Roshydromet meteorological station continuously operating at the island (**Figure 1**). There are no other anthropogenic constructions on the island. Thus, the major advantage of a new-developed research station is its long distance from any local anthropogenic sources. Previous research at the Tiksi station has shown significant aerosol pollution from local sources (Popovicheva et al., 2019), which is not the case in the "Island Bely" station. An aerosol sampling system was installed at the aerosol pavilion in May 2019. Three total suspended particle (TSP) inlets were installed approximately 1.5 m above the roof and 4 m above the ground. One is used for the real-time BC monitoring with air flow 5 L/min, and two for aerosol chemical characterization operating with 2.3 m^3/h flow. The TSP inlet is equipped with an electric heating wire to prevent rimming and ice blocking of the system.

Deleted: Figure 1
Deleted: Figure 1
Deleted:

An Aethalometer model AE33 (Magee Scientific,Aerosol d.o.o.) was used to measure the light attenuation caused by particles depositing on two filter spots at different flow rates (Drinovec et al., 2015) and at seven wavelengths from ultraviolet (370 nm) to infrared (950 nm). The "dual spot" technique is applied for real-time loading effect compensation. The light-absorbing content of carbonaceous aerosol at 880 nm is reported as equivalent black carbon concentration (EBC),

which is determined for each time interval from the change in the light attenuation at a wavelength of 880, using a mass absorption cross-section of 7.7 m^2/g and filter multiple scattering parameter C of 1.57. Light absorbing organic components (BrC) absorb light at shorter wavelengths more effectively than at 880 nm, which is observed as an increased AAE (Sandradewi et al., 2008; Grange et al., 2020; Helin et al., 2021). AAE was calculated using Eq. 1 for 470 nm and 950 nm wavelengths:

$$AAE = \frac{\ln (babs(470)/babs\,(950))}{\ln (950/470)} \quad (1)$$

where b_{abs} stands for the absorption coefficient at 470 nm and 950 nm. In order to avoid instrumental noise when calculating the AAE, the following data processing was implemented. One-minute absorption coefficients for the whole period were averaged to 1 hour. The dataset was filtered to periods when EBC exceeded 20 ng/m^3 (sensitivity level at 1 hour time resolution), and then the AAE was averaged to 3 hours.

The Aethalometer model (Sandradewi et al., 2008) is typically used for the source apportionment of EBC, when measurements of absorption coefficient are performed by filter photometers. The model uses an apriori assumed pair of AAE for traffic (AAETR) and biomass burning (AAEBB) to determine the contribution of both sources. Although the Aethalometer model is an efficient tool for source apportionment of EBC in a well-mixed urban atmosphere, where two sources with distinct aerosol optical properties prevail (fossil fuel from traffic and fresh biomass burning), the results can be affected when the characteristic optical properties of a specific source change over time. This is usually the case for wildfires, where different burning modes (flaming or smoldering) and different types of wood can significantly influence BrC emissions and its chemical composition (Kalogridis et al., 2018b). Furthermore, chemical evolution after emissions and atmospheric aging (i.e. aerosol mixing state, particle morphology and size distribution) additionally influence aerosol absorption, which can be noticed especially for long-range transported air masses (Cappa et al., 2016; Saleh et al., 2013; Romshoo et al., 2021). (Forrister et al., 2015) have shown that BrC emitted from wildfires was highly unstable, with 6% of BrC remaining above background levels after two days.

BC measurements at the "Island Bely" station were performed from 10 August 2019 to 30 November 2020, with a time resolution of 1 min. Basic meteorological parameters, such as temperature, wind speed and direction were obtained every 3 hours from a meteorological station located 500 m from the "Island Bely" station. Cleaning of 1-min time resolved BC data was based on the definition of what can be considered as a peak: strong fast increase of BC value a few times higher than previous value and then a similar fast decrease. Analysis of meteorological parameters

Deleted:
Formatted: Superscript
Deleted: calculated
Deleted: from
Deleted: -
Deleted: averaged dataset
Deleted: model
Deleted: true
Deleted: with
Deleted: the
Deleted: the
Deleted: the
Deleted: However, the remaining increase over the background can importantly influence the radiative forcing in the Arctic environment.
Moved (insertion) [1]
Deleted: The b
Deleted: by

was complementary to check whether the wind originated from the sector corresponding to locations of diesel generators at the Roshydromet meteorological station (240-250 degrees from the "Bely Island" station). In such cases, strong peaks of BC were removed from further analysis. The total duration of the peaks under the influence of local contamination varies from several minutes to one–two hours per day and monthly. For instance, in January 2020, when wind blew from 240-250 degrees for 24 hours in total, large peaks corresponding to a fraction of 13% of the data were removed. In July 2020, when wind originated from the same location for a total of 45 hours, measurements corresponding to a fraction of 22% of the data were removed. Lack of windy weather at Bely Island is a very rare event, only 0.7% of the observation time; during such weather, peaks of BC were never observed.

2.2 Atmospheric transport model coupling with emissions

To investigate the possible origin of BC, the Lagrangian particle dispersion model FLEXPART (FLEXible PARTicle dispersion model) version 10.4 was used (Pisso et al., 2019). The model was driven by 3-h operational meteorological fields from the European Centre for Medium-Range Weather Forecasts (ECMWF) with 137 vertical levels and a horizontal resolution of 1°×1°. In FLEXPART, computational particles were released at height 0 - 100 m from the receptor ("Island Bely" station) and were tracked backward in time in FLEXPART's "retroplume" mode. Simulations extended over 30 days backward in time, sufficient to include most BC emissions arriving at the station, given a typical BC lifetime of 1 week (Bond et al., 2013).

The tracking includes gravitational settling for spherical particles of the size observed. FLEXPART differs from trajectory models due to its ability to simulate dry and wet deposition of gases or aerosols (Grythe et al., 2017), turbulence (Cassiani et al., 2015), unresolved mesoscale motions (Stohl et al., 2005), while it includes a deep convection scheme (Forster et al., 2007). For our simulations, we assumed that BC has a density of 1500 kg m^{-3} and follows a logarithmic size distribution with an aerodynamic mean diameter of 0.25 μm and a logarithmic standard deviation of 0.3 (Long et al., 2013) .

FLEXPART simulations were performed every 3 hours during the studied period. The FLEXPART output consists of a footprint emission sensitivity which results in a modelled concentration at the receptor, when coupled with gridded emissions from an emission inventory. The emission sensitivity expresses the probability of any release occurring in each grid-cell to reach the receptor. The source contributions to receptor BC were derived by combining each gridded emission sector (e.g. gas flaring, transportation, waste management etc…) from an emission inventory with the footprint emission sensitivity. Calculations for anthropogenic sources

Deleted: For screening the BC data, we used the measured wind direction.

Deleted: that

Deleted: BC spikes

Deleted: that coincided with wind directions related to local diesel sources

Deleted: data

Deleted: e

Moved up [1]: The basic meteorological parameters, such as temperature, wind speed and direction were obtained every 3 hours by a meteorological station located 500 m from the "Island Bely" station.

Deleted: ourly

Deleted: n

Deleted: yields

Deleted: simulated

Deleted: in

Deleted: box

Deleted: can also be interpreted as a

Deleted: distribution field of the particle origin

Deleted: Arctic

Deleted: incorporating

Deleted: the

Deleted: retention time into the column emission flux

Deleted: , which was adopted

Deleted: the

Deleted: ies in each grid-cell

(emission sectors are described below) and open biomass burning were performed separately. This enabled identification of the exact origin of BC and allowed for quantification of its source contribution. The modelled concentrations can also be displayed as a function of the time elapsed since the emission has occurred (i.e., ”age”), which can be shown as “age spectrum”.

In this study, anthropogenic emission fluxes were adopted from the lastest version (v6b) of the ECLIPSE (Evaluating the CLimate and Air Quality ImPacts of ShortlivEd Pollutants) dataset, an upgraded version of the previous version (Klimont et al., 2017). The inventory includes industrial combustion (IND) emissions from industrial boilers and industrial production processes. Energy production sector (ENE) includes emissions from combustion processes in power plants and generators. Residential and commercial sector (DOM) includes emissions from combustion in heating and cooking stoves and boilers in households and public and commercial buildings. Waste treatment and disposal sector (WST) resembles emissions from waste incineration and treatment. Transport sector (TRA) includes emissions from all land-based transport of goods, animals and persons on road networks and off-road activities. Emissions from shipping activities in in-land waters (SHP) is included as a separate sector. Gas flaring (FLR) sector includes emissions from oil and gas facilities. The methodology for obtaining emissions from FLR specifically over Russia has been improved in ECLIPSEv6 (Böttcher et al., 2021). Updates were based on new field-type specific emission factors that were applied to VIIRS observations of the flared gas volume at individual flaring locations. For comparison, BCRUS emissions for the FLR sector (Huang et al., 2015) were also used in this study.

Emissions from biomass burning (BB) were adopted from Copernicus Atmosphere Monitoring Services (CAMS) Global Fire Assimilation System (GFAS). CAMS GFAS assimilates fire radiative power (FRP) observations from satellite-based sensors converting the energy released during fire combustion into gases and aerosol daily fluxes (Di Giuseppe et al., 2016; Kaiser et al., 2012). Data are available globally on a regular grid with a horizontal resolution of 0.1 degrees from 2003 to the present. FRP observations assimilated in GFAS are the NASA Terra MODIS and Aqua MODIS active fire products (http://modis-fire.umd.edu/, (Kaufman et al., 2003). FRP measures the heat power emitted by fires, as a result of the combustion process and is directly related to the total biomass combusted (Wooster et al., 2005). Using land-use-dependent conversion factors, GFAS converts FRP into emission estimates for 44 smoke constituents (Kaiser et al., 2012), one of which is BC.

Biomass burning emissions were also adopted from the Global Fire Emission Dataset version 4.1 (GFEDv4.1). The product combines satellite information on fire activity and vegetation productivity to estimate gridded monthly burned area and fire emissions, as well as

Deleted: different

Deleted: source contribution

Deleted: of

Deleted: . We used

Deleted: emissions in this study

scalars that can be used to calculate higher temporal resolution emissions. All data are publicly available for use in large-scale atmospheric and biogeochemical studies and include (i) burned area (Giglio et al., 2013) , (ii) burned area from "small" fires based on active fire detections outside the burned area maps detailed in (Randerson et al., 2012) and updates in (Werf et al., 2017), (iii) carbon and dry matter emissions from van der Werf et al. (2017), (iv) fractional contributions of various fire types to total emissions and (v) list of emission factors to compute trace gas and aerosol emissions based on (Akagi et al., 2011) and (Andreae and Merlet, 2001). The current version (v4) has a spatial resolution of 0.25 degrees and is available from 1997 onwards.

In the present paper, several different configurations were used to calculated modelled surface BC concentrations at "Island Bely" station, namely ECLIPSEv6 with GFED4 (ECLIPSEv6-GFED4), and ECLIPSEv6 with CAMS (ECLIPSEv6-CAMS). The same two configurations were also used after substituting the FLR emissions in ECLIPSEv6 with those from BCRUS (Huang et al., 2015).

3 Results and discussion

3.1 Monthly climatology of black carbon

The climate at the Bely Island is characterized by an average annual temperature of -8°C, precipitation of 450 mm, and stable snow coverage from October to May. Meteorology displays a large annual variability determined by alternating periods of the polar night and midnight sun. Median temperatures stay above 0ºC for 4 months each year between June and September. This period is also characterized by the highest-frequency occurrence of ocean air masses and the most stable wind speeds. A shift occurred in October with decreased solar insolation resulting in a temperature shift to below 0ºC. The cold month winds were primarily continental, with a low-frequency occurrence of ocean air masses.

The cycle of temperature and wind speed variations observed during the study period is shown in Figure 2a,b. The period from 1 November 2019 to 1 April 2020, when temperature dropped below -10 ^{0}C, as well as November 2020, is denoted as the "cold period". The remaining period of our study, from 10 August to 31 October 2019 as well as from April to 1 November 2020, is considered as the "warm period". Figure 2c illustrates the long-term time series of 24h median EBC concentrations measured at wavelength of 880 nm (EBC(880)) during the study period, with median value 37±64 ng/m^3 (maximum: 520 ng/m^3, minimum: 6 ng/m^3). The polar frequency plot of wind speed/direction shows that the maximum number of hours the wind was from north-east and south-west directions with around 5 m/s (Figure 3a). BC concentration roses

Deleted: the
Deleted: Figure 2
Deleted: Period
Deleted: in the present paper.
Deleted: Figure 2
Deleted: ,
Deleted: and minimum of
Deleted:
Deleted: and
Deleted: , respectively
Deleted: s
Formatted: Font: Not Italic
Deleted: Figure 3

in **Figure 3** indicate the sources of the highest concentrations, which originated from the continent in both cold and warm periods.

Figure 4 illustrates a long-term time series of monthly EBC concentrations at the "Island Bely" station during the period from August 2019 to November 2020. The highest concentrations were observed from November to April and the lowest ones from June to August, in agreement with the typical seasonal trend of the Arctic aerosol concentrations (Stone et al., 2014). EBC monthly climatology during the study period is shown in **Figure 4**a in terms of the median, and upper and lower quartiles. For winter months, the maximum median EBC concentration was 165 ng/m^3 observed in December 2019. The increase of the Arctic concentrations in winter, known as the Arctic Haze, was more pronounced in November-December 2019 and January-March 2020. On average, concentrations in summer were about 10 times lower than those in winter, with a minimum median value of 30 ng/m^3 in July 2020. Observations at the "Island Bely" station for the second year started from August 2020 and lasted to November 2020 to confirm the general annual trend of low summer and high winter BC concentrations. However, monthly median EBC in September 2020 demonstrated a value of 30.7 ng/m^3.

Similar annual trend was recorded in 2015-2016 at the Tiksi station (coast of Laptev sea), with high concentrations reaching 130 ng/m^3 during winter-spring and low concentrations of about 20 ng/m^3 observed from May to October (Popovicheva et al., 2019b). As shown by earlier studies at various polar stations, such as in Ny-Ålesund, Alert, and Barrow, aerosols display Arctic Haze peak concentrations during winter and early spring months (Stone et al., 2014). EBC during Arctic Haze at both "Island Bely" and Tiksi stations are typically higher as compared to those observed at Alert (100±65 ng/m^3), a station that has shown the largest concentrations among all Polar stations (Sharma et al., 2004). The latter confirms previous findings from (Eckhardt et al., 2015) and (Winiger et al., 2017) that the Siberian Arctic is mainly polluted as a result of the influence from emissions occurring in the Eurasian continent.

Near-surface measurements allow for evaluation of the capability of transport models to reproduce the distribution of BC in the Arctic based on different emission datasets (Schacht et al., 2019; Zhu et al., 2020). **Figure 4**a and Supplentary Table S 2 show observed and modelled BC monthly median mass concentrations at the "Island Bely" station. Use of ECLIPSEv6 emissions caused overestimations of modelled BC concentrations of up to 46% (February 2020). All simulated BC concentrations were found in the range between the 25th and 75th percentiles of measured EBC. Modelled BC is underestimated in March-May 2020, being 29 ng/m^3 below the 25th percentile of EBC in April 2020. When FLR emissions in ECLIPSEv6 were substituted by BCRUS FLR, similar modelled BC monthly median concentrations were calculated, thus

Formatted: Font: Not Italic
Deleted: Figure 3
Formatted: Font: Not Italic
Deleted: Figure 4
Formatted: Indent: First line: 1 cm
Deleted: EBC
Deleted: Figure 4
Deleted: ¶
Deleted: of
Deleted: the unprecedented high
Deleted: 72
Deleted: , twice as much as in September 2019
Deleted: found
Deleted: in comparison
Deleted: ones
Deleted: which
Deleted: maximum
Deleted: due to
Deleted: of emissions
Deleted: the
Deleted: a
Deleted: Figure 4
Deleted: 1
Deleted: the
Deleted: flaring

indicating that other sectorial emissions might have a large contribution to surface BC at the station.

Figure 4b shows the so-called "age spectrum" of modelled BC for the "Island Bely" station. In the cold period of high EBC concentrations, the longest age of more than 19 days back, affects up to 60% of the surface concentrations. In this time, due to the geographical proximity, Russia dominates. However, both Europe and Asia contribute around 20% to the monthly averaged surface BC, with the largest contribution to be in February 2019 and November 2020, (**Figure 4**b,d). The most aged air masses (from 28 to 30 days back) contributed up to 50%, arriving at the "Island Bely" station in December 2019, which is the month of the highest observed EBC concentrations during the study period. The impact of the closest regions with age between 7 and 9 days is more significant in the winter months, while in the warm period, such short-term contributions become negligible. The calculated age and continental spectrum of BC obtained for the "Island Bely" station mainly denote the variability of airmass transport patterns in different seasons. In the cold season, the Siberian Arctic tends to force the air from south to north into the Arctic (Stohl, 2006), thus bringing more anthropogenic BC from highly populated regions.

Monthly averaged BC contributions from different sources simulated by FLEXPART using ECLIPSEv6 emissions are shown in **Figure 4**c and Supplementary Table S 3. From November 2019 to March 2020 the FLR sector contributed 47%–68% (maximum in January 2020) to surface BC, when air masses arrived at Bely through oil and gas extraction sites. February and November 2020 demonstrated the biggest non-gas flaring impact. More specifically, February 2020 coincides with the largest model overestimation (**Figure 4**a) implying a likely misestimation of non-gas flaring emissions in ECLIPSEv6. From April 2020 the impact of FLR dropped significantly (Supplementary Table S 4), with minimum of 12% in June. Starting from April to October 2020, BB emissions played the biggest role in surface BC, contributing 81% in July 2020. It is noteworthy that the impact of SHP emissions became quite perceptible in the warm period, when the oceanic ice is absent in the Arctic and touristic cruises peak.

Emission sensitivities of surface BC presented over the whole Arctic (north of 66°N) have been also simulated using the same model (Zhu et al., 2020). Anthropogenic sources contributed 82% of the annual BC, as estimated from BCRUS emission dataset. Arctic BC originated predominantly from anthropogenic emissions in Russia (56%), mainly FLR from YNAO, Khanty-Mansiysk Autonomous Okrug (KMAO), and Komi Republic (31% of surface Arctic BC). In summer (July-August), open BB in Siberia, Alaska, and Canada contributed 75%. At Zeppelin, modelled BC (39.1 ng/m^3 for annual mean) was reported to be 85% higher than the observed value (21.1 ng/m^3 for annual mean) (Zhu et al., 2020). At Tiksi, modelled BC was underestimated (74.4

Deleted: "Island Bely"

Deleted: FLEXPART simulations that extended over 30 days back in time can be displayed as a function of the time elapsed since the emission has occurred (age spectrum).

Deleted: Figure 4

Deleted: the contribution of a certain age (days backwards) estimated

Formatted: Indent: First line: 1.25 cm

Deleted: BC

Deleted: ;

Deleted: h

Deleted: biggest

Deleted: Figure 4

Deleted: the

Deleted: st

Deleted: ¶

Deleted: northward

Deleted: with

Deleted: Figure 4

Deleted: 2

Deleted: the

Deleted: Island

Deleted: , indicating that air masses passed through highly populated regions

Deleted: Especially

Deleted: ,

Formatted: Font: Not Italic

Deleted: Figure 4

Deleted: ,

Deleted: 3

Deleted: contribution,

Deleted: approaching

Deleted: June

Deleted: distinguished

Deleted: a

Deleted: cover

Deleted: as in the present in

Deleted: with

Deleted: being the main source

Deleted: Arctic

Formatted: English (US)

Deleted: the

Deleted: station

ng/m^3 for annual mean) by 40% compared with observations (104.2 ng/m^3 for annual mean) (Zhu et al., 2020). Annual (from September 2019 to August 2020) median modelled concentrations of BC using ECLIPSEv6, BCRUS, and CAMS for the "Island Bely" station are shown in Supplementary Table S 2. We find that modelled BC (78.4 ng/m^3 for annual mean) is 26% higher than the observed value (61.8 ng/m^3 for annual mean); the overestimation is much smaller than observed for other remote stations. Annual averaged contributions of anthropogenic emissions by ECLIPSEv6 and ECLIPSEv6 with flaring from BCRUS were equal to 76% and 80%, respectively, due to the difference in FLR emissions in the two datasets (Supplementary Table S 4).

3.2 Cold season pollution

Figure 5a shows EBC concentrations measured at the "Island Bely" station during the cold period, from November 2019 to April 2020 and from 1st to 30th November 2020. Time series indicates that EBC undergoes the Arctic-typical seasonal trend with higher concentrations in winter and early spring and lower in summer. Background pollutant concentrations in Arctic stations are generally very low without any detectable influence from local or regional sources (Eleftheriadis et al., 2004; Popovicheva et al., 2019b). We relate the Arctic background to the lowest 20th percentile of EBC data (10 ng/m^3). Long-term pollution episodes were assumed to be repeated events of high EBC concentration above the 80th percentiles (90 ng/m^3) that are clearly distinguishable from the background (**Figure 5**a).

The aerosol optical properties with respect to absorption, presented as daily median AAE is shown in **Figure 2**d. The AAE for highly aged aerosols measured during periods of low BC was lower than 1 (reaching values as low as 0.2) and is mostly related to the aerosol size distribution (large particles) and internally mixed BC particles (Cappa et al., 2016). As shown by modeling studies (Virkkula, 2021), pure BC particles surrounded by non-absorbing coatings can have AAE in the range from <1 to 1.7, also depending on the morphology of the fractal aggregates (Romshoo et al., 2021). The AAE increased in periods of higher aerosol concentration levels in the cold period ranging from 0.6 to 1.35.

In many cases, when AAE exceeded 1 in the cold period, the pollution episodes could be identified as influenced by BB. However, due to the mixing with background aerosol and aging processes, a large variability in AAE values might be observed at receptors of long range transported pollution and AAE may not be representative of BB sources. Nevertheless, it can still be used as a qualitative parameter, when extra information is available. Such events of increased AAE were rarely observed in our study, and the most prominent BB impact occurred during the pollution episodes C4, C7, and C8 when impact of domestic sources was significant (**Figure 5**a).

Deleted: in comparison with th
Deleted: e
Deleted: l
Deleted: in conjunction with the respective contribution of the…
Deleted: sector
Deleted: from
Deleted: l
Deleted: 3
Deleted: **Figure 5**
Deleted: as well as
Deleted: characteristic
Deleted: Arctic
Deleted: the
Deleted: of
Deleted: pollution
Deleted: ,
Deleted: **Figure 5**
Deleted: are
Deleted: **Figure 2**
Deleted: the
Deleted: the
Deleted: ,
Deleted: ,
Deleted: which is addressed
Deleted: coated
Deleted: also
Deleted: becomes more reliable
Deleted: , when it ranged
Deleted: When
Deleted: periods
Deleted: can
Deleted: Due
Deleted: e
Deleted: the air mass influenced by BB events is expected to have increased AAE as compared to BC produced by fossil fuel. However, ageing processes may induce
Deleted: high
Deleted: observed
Deleted: area
Deleted: P4
Deleted: P
Deleted: P
Deleted: the most prominent
Deleted: **Figure 5**

In general, FLEXPART coupled with ECLIPSEv6-CAMS emissions captures periods with both high and low concentrations relatively well, (**Figure 2**c). A good correlation between measurements and simulations, with a Pearson coefficient R of 0.7 and the root mean squared error (RMSE) of 89.2 ng/m^3 was obtained for the cold period (**Figure 6**a). According to monthly median contributions to BC concentrations in the cold period, the impact of anthropogenic sources, namely FLR, DOM and TRA dominated surface BC by 97.7% (**Figure 4**c).

Looking closely to specific episodes, during pollution episode C1, three events of high EBC concentrations were observed, (**Figure 5**a). On 5 November 2019, measured EBC reached 180 ng/m^3, while FLEXPART simulated similarly high BC values. Footprint emission sensitivities at this time showed that airmasses originated from East and North Europe, passed south of European Russia, then turned the direction straight through the West Siberia approaching the Bely Island from the southeast (**Figure 7**). The same airmassed moved towards the large Russian FLR sources of YNAO, KMAO, and Krasnoyarsky Krai (see **Figure 1**) causing up to 71% contribution to surface BC (Supplementary Table S 5).

On 12 November 2019, airmasses arrived at the Bely Island through the Yamal peninsula after passing from the ocean (Supplementary Figure S 1). Model strongly underestimated measured EBC concentrations by about 10 times (**Figure 7**). We fail to provide a concrete explanation for this; a simplified hypothesis is that a number of flaring sites located at the Yamal peninsula might have not been included into the emission database, but this certainly needs further research. In contrast, the model strongly overestimated measured EBC concentrations on 16 November 2019. At that time, airmasses passed through remote regions of Eastern Siberia and arrived through the gas flaring sites of Krasnoyarsky Krai at the station (**Figure 7**) causing an FLR contribution of 98.6% to surface BC (Supplementary Table S 5). The reason might be use of incorrect emission factors for BC at the FLR facilities of Krasnoyarsky Krai in the adopted emissions, because direct transport from this region was observed. During 12 and 16 November 2019 the AAE was in the range from 0.7 to 1, which agrees with the expected optical properties for the FLR sources.

Pollution episode C2 in December 2019 gave the highest EBC concentrations observed during the whole cold period, (**Figure 5**a). On 4 December, EBC approched 400 ng/m^3, when airmasses originated from Kazakhstan and Russian gas flaring regions of KMAO and YNAO (**Figure 8**). The maximum EBC concentration of approximately 500 ng/m^3 with AAE 1.05 was observed on 19 December, when air came from Europe, initially through the Russian oil and gas basins of Volga-Ural at the south of European Russia and then through KMAO and YNAO in

Deleted: Generally
Deleted: Figure 2
Deleted: ,
Deleted: is
Deleted: Figure 6
Deleted: Figure 5b
Deleted: P1
Deleted: Figure 5
Deleted: Figure 7
Deleted: is
Deleted: Figure 1
Deleted: 4
Deleted: Figure 7
Deleted: fields
Deleted: Figure 7
Deleted: 4
Deleted: P2
Deleted: Figure 5
Deleted: Figure 8
Deleted: reached the Bely Island
Deleted: was

Western Siberia (**Figure 8**). During the December pollution events, FLR contribution dominated, reaching 73% on 19 December (Supplementary Table S 5).

The highest FLR contributions were observed during the pollution episodes C3–C6 (Supplementary Table S 5). Similar airmass transportation through either gas and oil fields of YNAO and KMAO in Western Siberia or Komi and Nenets regions north of European Russia occurred in all of the events, (Supplementary Figure S 1).

In contrast to the aforementioned events, the pollution episode C7 was unrelated to FLR, as airmasses did not cross flaring regions (**Figure 8**). On 16 November 2020, retroplumes confirm origin of surface BC from Central and Eastern Europe and the Kola Peninsula (**Figure 8**). DOM and TRA hold the largest share of the source contribution with 73% and 20%, respectively (Supplementary Table S 5), while the model overestimated measured EBC. Episode C8 gave the biggest EBC (370) concentration which reached 346 ng/m^3 and exceeded EBC (880) (133 ng/m^3) on 24 November 2020 (Supplementary Table S 5). At this time, airmasses came to the Bely Island directly from the most populated region of European Russia (**Figure 8**). The contribution of DOM and TRA was 34% and 23%, respectively. AAE approached the highest value observed (1.3) during the study period. This might show a detectable impact of biomass burning in the classified DOM emissions. BC from wood burning contributes around 61% of the total residential emissions, especially in areas where there is limited use of natural gas (Kalogridis et al., 2018a), and in forest regions (Huang et al., 2015). Note that the impact of IND emissions was the largest in episodes C7 and C8 as compared to the whole cold period (Supplementary Table S 5), due to industrial emissions from sites in Central European Russia.

3.3 Warm season pollution

Figure 5b shows EBC concentrations measured at the "Island Bely" station during the warm period, from 10 August to 31 October 2019 and from 1 April to 1 November 2020. It is immediately seen that BC in the warm period was mainly affected by Russian emissions (90%), and only in October 2020 and August 2019 partly (~20%) from Europe and North America, (**Figure 4**). EBC concentrations rarely exceeded the 80th percentile that was set as the pollution criterion, while the duration of the warm period episodes was shorter.

Due to the mixing with background aerosol and aging processes, airmasses influenced by BB events should be expected to have increased AAE as compared to the BC produced by fossil fuel. However, aging processes may induce a high variability in AAE in areas affected by long-range transport, and hence AAE may not be representative of a BB source. Pollution events were

Deleted: Figure 8
Deleted: 4
Deleted: P3
Deleted: -
Deleted: P
Deleted: 4
Deleted: for
Deleted: P7
Deleted: the
Deleted: Figure 8
Deleted: the
Deleted: Figure 8
Deleted: 4
Deleted: P8
Deleted: 4
Deleted: at
Deleted: part of
Deleted: Figure 8
Deleted: us, it
Deleted: addresses
Deleted: P
Deleted: P
Deleted: events
Deleted: 4
Deleted: Figure 5
Deleted: Figure 4
Deleted: e
Deleted: the
Deleted:
Deleted: is
Deleted: e
Deleted: at receptor
Deleted: of
Deleted: ed
Deleted: pollution and the
Deleted: aerosol
Deleted: It is used here as a qualitative tool.

rarely observed in this season, and the most sufficient BB impact occurred during the pollution episodes W4, W7, and W8.

However, events characterised by higher AAE were observed more often indicating that BB impact was more significant during the warm period, mainly during spring and summer (episodes W3, W4, and W6). Comparison between measured and modelled concentrations showed poor correlation (R of 0.41 and RMSE of 121 ng/m^3) (**Figure 6**). According to monthly median contributions to surface BC concentrations in the warm period, the impact of BB emissions was as high as 50% (**Figure 4**c). SHP emissions contributed about 1%, as a result of the increase of touristic activity in the Arctic and the more active use of the Northern Sea Route due to the Arctic ice retreat.

From the beginning of the study period in August 2019, large wildfires were observed in Siberia (Voronova et al., 2020). The latter resulted in a strong BB impact at the "Island Bely" station (**Figure 5**b). However, during episode W1, EBC concentrations reached approximately 200 ng/m^3 not caused by wildfire plumes (**Figure 5**). During this time, airmasses were transported from Northern Europe (Supplementary Figure S 1), and the main contribution to surface BC at the "Island Bely" station was due to TRA emissions (36%, Supplementary Table S 5).

Episode W2 during October 2019 (**Figure 5**) was characterised by EBC of 119 ng/m^3, while modelled BC was strongly overestimated (Supplementary Figure S 1). The calculated BB contribution to station's surface BC was 64% (Supplementary Table S 5) and the hotspot BB sources were near the Pur River (YNAO), as recorded by CAMS (Supplementary Figure S 1). The measured AAE does not indicate any contribution from BrC, as it would be expected for BB sources and observed AAE values were lower than 1 (Supplementary Table S 5). Note that the FIRMS active fire data analyses (https://firms.modaps.eosdis.nasa.gov/) indicate that the fire spots were in the same grid-cell as industrial facilities of oil extraction field in the Purovski region (YNAO). Thus, it might be that thermal anomalies from flaring facilities were mistakenly related to fires in CAMS. This hypothesis is reinforced by the fact that no wildfires were recorded by the local forest fire service (https://aviales.ru) during October 2020 in Western Siberia and Krasnoyarsky Krai.

Pollution episode W3 is related to a strong springtime wildfire activity that occurred in Southern Siberia. The retroplumes on 18 and 23 April 2020 showed that the air originated from Central Asia, a large territory of Southern Siberia and Krasnoyarsk Kray, and arrived at the Bely Island through the Western Siberia from the southeast (Supplementary Figure S 1, **Figure 9**). High footprint emission sensitivities coincided with the location of large wildfires resulting in BB

Deleted: prominent
Deleted: P4
Deleted: P
Deleted: P
Deleted: the
Deleted: frequently
Deleted: ,
Deleted: the
Deleted: of BB
Deleted: P3
Deleted: P
Deleted: P
Deleted: **Figure 6**
Deleted: **Figure 4**
Deleted: into the Arctic BC
Deleted: **Figure 5**
Deleted: c
Deleted: event
Deleted: P
Deleted: the observed
Deleted: of
Deleted: were
Deleted: the
Deleted: **Figure 5**
Deleted: the
Deleted: 4
Deleted: P2
Deleted: **Figure 5**
Deleted: high
Deleted:
Deleted: .
Deleted: M
Deleted: concentrations
Deleted: ere
Deleted: the
Deleted: 4
Deleted: of
Deleted: , which
Deleted: .
Deleted: observed during the P2 episode
Deleted: 4
Deleted: P3
Deleted: ing
Deleted: **Figure 9**

contribution to surface BC at the station equal to 28% (18 April 2020) and 19% (23 April 2020), respectively. The most significant impact of wildfires was observed on 23 April 2020, when 6-h median EBC concentration reached 700 ng/m3 with AAE ranging from 1.3 to 1.5, clearly indicating an elevated contribution of BrC (Supplementary Table S 5).

Wildfires occurred in northern Krasnoyarsk Krai and Sakha Republic, Central Siberia between April and November 2020 (https://aviales.ru/popup.aspx?news=6286) that burned around seven million hectares of forest. The pollution episode W4 on 7 July 2020 recorded a 6-h median EBC of 150 ng/m^3 and an AAE of around 1.4 clearly indicating BB impact. The model captures this event well, providing the highest BB contribution exactly when observed, equal to 90% (Supplementary Table S 5). Airmasses arrived from the east and passed north of Krasnoyarsk Kray where the large wildfires occurred (**Figure 9**).

Unprecedented high wildfire-related BC concentration was observed in September 2020 (pollution episode W6). EBC concentrations exceeded 5 and 20 times the 80th percentile of the measurements. Maximum 6-h median EBC reached 534 ng/m^3 on 1st September 2020 and it was even higher than the biggest Arctic haze concentration observed in December 2019, (Supplementary Table S 5). Increased AAE of around 1.4 revealed strong BB impact. This event resulted from long-range transport of BC from the Eurasian continent during the intensive wildfires in Western Siberia (Krasnoyarsk Kray and Yakutia) (**Figure 9**), where around one million hectares of forest were burned in August 2020. The contribution of BB to surface BC at the "Island Bely" station was as high as 95%.

Despite the exclusive BB origin of the light absorbing carbon measured at the "Island Bely" station, the AAE was much lower than the established value for fresh BB (close to 2) (Sandradewi et al., 2008) likely due to aging. This apparent reduction of the BrC contribution to absorption is in agreement with (Forrister et al., 2015), who examined BrC concentrations and AAE from Western U.S. forest fires as a function of aging. Their results show that most of the BrC (~94%) emitted from wildfires was lost within a day. Similar observations have been reported for long-range transported North American smoke over the Northeastern Atlantic (Zheng et al., 2020) and for transported Russian smoke over the Mediterranean (Diapouli et al., 2014).

The last pollution episode W7 was observed at the end of October 2020. Although it occurred in the warm period, it is rather related to Russian FLR and European TRA emissions (Supplementary Table S 5, **Figure 5**b). At the end of October 2020 airmasses came mainly from Europe, passing through the Yamal Peninsula.

4 Conclusions

Deleted: "Island Bely"
Deleted: our
Deleted: 4
Deleted: burning
Deleted: P4
Deleted: was recorded at the "Island Bely" station
Deleted: , with
Deleted: ,
Deleted: 4
Deleted: Figure 9
Deleted: P6
Deleted: that
Deleted: 4
Deleted: indicted prominent
Deleted: Such a strong
Formatted: Font: Not Italic
Deleted: Figure 9
Deleted: ; there,
Deleted: is
Deleted: e
Deleted: ich
Deleted: of
Deleted: s
Deleted: long range
Deleted: P7
Deleted: 4
Deleted: Figure 5

The present paper aims at performing a quantitative analysis of the Arctic pollution via high-resolution measurements from a recently developed aerosol station at the Bely Island (Kara Sea) combined with Lagrangian modelling. A consequent goal is to examine the impact of anthropogenic and natural sources to the high Arctic as a result of long-range transport. The main results can be summarised as follows:

- EBC monthly climatology is following the typical Arctic aerosol seasonal variation characterised with higher EBC concentrations in winter and lower in summer.
- AAE for aged BC larger than 1 indicates wildfire impact in the warm period, but mixing with gas flaring emissions from nearby regions was also observed.
- The recently upgraded ECLIPSEv6 emissions and ECLIPSEv6 coupled with FLR from BCRUS represent measured EBC accurately in the cold period. Annual average contributions of anthropogenic emissions to surface BC were 76% and 80% (50% and 59% from gas flaring) for each dataset, respectively.
- The most significant model overestimation was observed in February 2020, when air masses passed through non gas flaring regions. The largest underestimation occurred in April 2020 during the period of spring agriculture fires.
- Daily BB emissions from CAMS were more efficient in representing pollution episodes than monthly GFED4 emissions, and therefore they were mainly used here.
- Russian emissions dominate during the whole year, European and Asian ones contribute up to 20% in the cold period. Pollution episodes with EBC concentrations above 90 ng/m^3 occur in 18.5% of observation time. Monthly average FLR emissions dominate (98%) any other emission sector.
- FLR and BB emissions contribute the largest share of EBC to the "Island Bely" station during the cold and warm period, respectively. This is consistent with previously-reported source contributions to the the Russian Arctic. When air is transported from Europe, other sources such as TRA become important. The same applies for SHP emissions that become important in summertime, because of cruise activities and ice retreat.
- Emissions from gas and oil fields in Western Siberia, and the Northern European Russia cause the vast majority of the pollution episodes in the Arctic.
- 15 pollution episodes with concentrations reaching close to 723 ng/m3 were detected. The duration of the cold pollution episodes is longer than of the warm period, and the median (up to 160 ng/m3) and maximum EBC (up to 450 ng/m3) concentrations higher.

In conclusion, the significance of high-quality measurements at the "Island Bely" station is pronounced from the present study, because (i) the station is located along the main pathway of

Deleted: between
Deleted: and 1.35
Deleted: wood burning impact from domestic activity and/or…
Deleted: s
Deleted: both periods
Deleted:
Deleted: examined
Deleted: flaring
Deleted: of total emissions
Deleted: observed
Deleted: in
Deleted: the
Deleted: part of
Deleted: 500
Deleted: in

airmasses entering the Arctic, and (ii) it is north of the world's largest gas flaring regions. The operation of the "Island Bely" station is an asset in source emission optimisation, because EBC measurements in the High Arctic are still rare.

Data availability. All model data used in the present publication together with all figures of footprint analysis and source contributions to surface BC are open through the websites https://niflheim.nilu.no/NikolaosPY/Bely_2020_cams.py and https://niflheim.nilu.no/NikolaosPY/Bely_2020_huang_cams.py. All row model data can be obtained from the corresponding author upon request. The definitions of the regions and continents used in the current analysis are based on regional masks that can be seen in Supplementary Figure S 3.

Competing interests. The authors declare no competing interests.

Acknowledgements. This research was performed in the frame of the Development program of the Interdisciplinary Scientific and Educational School of M. V. Lomonosov Moscow State University "Future Planet and Global Environmental Change". Authors wish to thank much Dr. Tony Hanson (Magee Scientific) for his support on the AE33 aethalometer installation and operation at the "Island Bely" station, as well as Dr. A. Sinitsky for organizational support.

Financial support. Development of the methodology for aethalometric measurements and AAE calculations was performed in the frame of RSF project #19 -77-30004. Aerosol infrastructure developing methodology was implemented under the RF Ministry of Science and Higher Education (agreement № 075-15-2021-938).All model and code developments and calculations were supported by the COMBAT (Quantification of Global Ammonia Sources constrained by a Bayesian Inversion Technique) project funded by ROMFORSK – Program for romforskning of the Research Council of Norway (Project ID: 275407, website: https://prosjektbanken.forskningsradet.no/project/FORISS/275407?Kilde=FORISS&distribution=Ar&chart=bar&calcType=funding&Sprak=no&sortBy=date&sortOrder=desc&resultCount=30&offset=0&ProgAkt.3=ROMFORSK-Program+for+romforskning) and the EC Horizon 2020 – Research and Innovation Framework Programme ATMO-ACCESS Integrating Activity under grant agreement No 101008004. The work was partly supported by the European Union's Horizon 2020 European research infrastructures programme ACTRIS-IMP under grant agreement No 871115.

Deleted: huge

Author contributions. O.B.P. supervised the station operation, interpreted data and wrote the manuscript. N.E. performed all the FLEXPART simulations and analyses, wrote and coordinated the paper. V.O.K. analyzed the data. M.A.C. prepared the figures and assisted in the interpretation of the results. K.E. provided BB impact and AAE aging evaluation. A.G. performed AAE calculations and evaluation of data quality. N.S.K. supported the research. All authors contributed to the final version of the manuscript.

References

Akagi, S., Yokelson, R. J., Wiedinmyer, C., Alvarado, M., Reid, J., Karl, T., Crounse, J., and Wennberg, P.: Emission factors for open and domestic biomass burning for use in atmospheric models, Atmospheric Chemistry and Physics, 11, 4039-4072, 2011.

Andreae, M. O. and Merlet, P.: Emission of trace gases and aerosols from biomass burning, Global biogeochemical cycles, 15, 955-966, 2001.

Bond, T. C., Doherty, S. J., Fahey, D., Forster, P., Berntsen, T., DeAngelo, B., Flanner, M., Ghan, S., Kärcher, B., and Koch, D.: Bounding the role of black carbon in the climate system: A scientific assessment, Journal of Geophysical Research: Atmospheres, 118, 5380-5552, 2013.

Böttcher, K., Paunu, V.-V., Kupiainen, K., Zhizhin, M., Matveev, A., Savolahti, M., Klimont, Z., Väätäinen, S., Lamberg, H., and Karvosenoja, N.: Black carbon emissions from flaring in Russia in the period 2012-2017, Atmospheric Environment, 118390, 2021.

Cappa, C. D., Kolesar, K. R., Zhang, X., Atkinson, D. B., Pekour, M. S., Zaveri, R. A., Zelenyuk, A., and Zhang, Q.: Understanding the optical properties of ambient sub- and supermicron particulate matter: results from the CARES 2010 field study in northern California, Atmos. Chem. Phys., 16, 6511-6535, 10.5194/acp-16-6511-2016, 2016.

Cassiani, M., Stohl, A., and Brioude, J.: Lagrangian stochastic modelling of dispersion in the convective boundary layer with skewed turbulence conditions and a vertical density gradient: Formulation and implementation in the FLEXPART model, Boundary-Layer Meteorology, 154, 367-390, 2015.

Chang, R.-W., Leck, C., Graus, M., Müller, M., Paatero, J., Burkhart, J. F., Stohl, A., Orr, L., Hayden, K., and Li, S.-M.: Aerosol composition and sources in the central Arctic Ocean during ASCOS, Atmospheric Chemistry and Physics, 2011.

Cho, M.-H., Park, R. J., Yoon, J., Choi, Y., Jeong, J. I., Labzovskii, L., Fu, J. S., Huang, K., Jeong, S.-J., and Kim, B.-M.: A missing component of Arctic warming: black carbon from gas flaring, Environmental Research Letters, 14, 094011, 2019.

Conrad, B. M. and Johnson, M. R.: Field measurements of black carbon yields from gas flaring, Environmental science & technology, 51, 1893-1900, 2017.

Di Giuseppe, F., Remy, S., Pappenberger, F., and Wetterhall, F.: Improving CAMS biomass burning estimations by means of the Global ECMWF Fire Forecast system (GEFF), ECMWF Tech. Memo. 790, 18 pp., https://www. ecmwf. int/sites/default/files …, 2016.

Drinovec, L., Močnik, G., Zotter, P., Prévôt, A., Ruckstuhl, C., Coz, E., Rupakheti, M., Sciare, J., Müller, T., and Wiedensohler, A.: The" dual-spot" Aethalometer: an improved measurement of aerosol black carbon with real-time loading compensation, Atmospheric Measurement Techniques, 8, 1965-1979, 2015.

Eckhardt, S., Quennehen, B., Olivié, D. J. L., Berntsen, T. K., Cherian, R., Christensen, J. H., Collins, W., Crepinsek, S., Daskalakis, N., Flanner, M., Herber, A., Heyes, C., Hodnebrog, Ø., Huang, L., Kanakidou, M., Klimont, Z., Langner, J., Law, K. S., Lund, M. T., Mahmood, R., Massling, A., Myriokefalitakis, S., Nielsen, I. E., Nøjgaard, J. K., Quaas, J., Quinn, P. K., Raut, J. C., Rumbold, S. T., Schulz, M., Sharma, S., Skeie, R. B., Skov, H., Uttal, T., von Salzen, K., and Stohl, A.: Current model capabilities for simulating black carbon and sulfate concentrations

in the Arctic atmosphere: a multi-model evaluation using a comprehensive measurement data set, Atmos. Chem. Phys., 15, 9413-9433, 10.5194/acp-15-9413-2015, 2015.
Eleftheriadis, K., Vratolis, S., and Nyeki, S.: Aerosol black carbon in the European Arctic: Measurements at Zeppelin station, Ny-Ålesund, Svalbard from 1998–2007, Geophysical Research Letters, 36, n/a-n/a, 10.1029/2008GL035741, 2009.
Eleftheriadis, K., Nyeki, S., Psomiadou, C., and Colbeck, I.: Background aerosol properties in the European arctic, Water, Air and Soil Pollution: Focus, 4, 23-30, 2004.
Flanner, M. G.: Arctic climate sensitivity to local black carbon, Journal of Geophysical Research: Atmospheres, 118, 1840-1851, 10.1002/jgrd.50176, 2013.
Forrister, H., Liu, J., Scheuer, E., Dibb, J., Ziemba, L., Thornhill, K. L., Anderson, B., Diskin, G., Perring, A. E., and Schwarz, J. P.: Evolution of brown carbon in wildfire plumes, Geophysical Research Letters, 42, 4623-4630, 2015.
Forster, C., Stohl, A., and Seibert, P.: Parameterization of convective transport in a Lagrangian particle dispersion model and its evaluation, Journal of applied meteorology and climatology, 46, 403-422, 2007.
Giglio, L., Randerson, J. T., and Van Der Werf, G. R.: Analysis of daily, monthly, and annual burned area using the fourth-generation global fire emissions database (GFED4), Journal of Geophysical Research: Biogeosciences, 118, 317-328, 2013.
Grange, S. K., Lötscher, H., Fischer, A., Emmenegger, L., and Hueglin, C.: Evaluation of equivalent black carbon source apportionment using observations from Switzerland between 2008 and 2018, Atmospheric Measurement Techniques, 13, 1867-1885, 2020.
Grythe, H., Kristiansen, N. I., Groot Zwaaftink, C. D., Eckhardt, S., Ström, J., Tunved, P., Krejci, R., and Stohl, A.: A new aerosol wet removal scheme for the Lagrangian particle model FLEXPART v10, Geosci. Model Dev., 10, 1447-1466, 10.5194/gmd-10-1447-2017, 2017.
Helin, A., Virkkula, A., Backman, J., Pirjola, L., Sippula, O., Aakko-Saksa, P., Väätäinen, S., Mylläri, F., Järvinen, A., and Bloss, M.: Variation of absorption Ångström exponent in aerosols from different emission sources, Journal of Geophysical Research: Atmospheres, 126, e2020JD034094, 2021.
Huang, K., Fu, J. S., Prikhodko, V. Y., Storey, J. M., Romanov, A., Hodson, E. L., Cresko, J., Morozova, I., Ignatieva, Y., and Cabaniss, J.: Russian anthropogenic black carbon: Emission reconstruction and Arctic black carbon simulation, Journal of Geophysical Research: Atmospheres, 120, 11,306-311,333, 2015.
Ismail, O. S. and Umukoro, G. E.: Global impact of gas flaring, Energy and Power Engineering, 4, 290, 2012.
Johnson, M. S., Strawbridge, K., Knowland, K. E., Keller, C., and Travis, M.: Long-range transport of Siberian biomass burning emissions to North America during FIREX-AQ, Atmospheric Environment, 252, 118241, 2021.
Kaiser, J., Heil, A., Andreae, M., Benedetti, A., Chubarova, N., Jones, L., Morcrette, J.-J., Razinger, M., Schultz, M., and Suttie, M.: Biomass burning emissions estimated with a global fire assimilation system based on observed fire radiative power, Biogeosciences, 9, 527-554, 2012.
Kalogridis, A.-C., Vratolis, S., Liakakou, E., Gerasopoulos, E., Mihalopoulos, N., and Eleftheriadis, K.: Assessment of wood burning versus fossil fuel contribution to wintertime black carbon and carbon monoxide concentrations in Athens, Greece, Atmospheric Chemistry and Physics, 18, 10219-10236, 2018a.
Kalogridis, A. C., Popovicheva, O. B., Engling, G., Diapouli, E., Kawamura, K., Tachibana, E., Ono, K., Kozlov, V. S., and Eleftheriadis, K.: Smoke aerosol chemistry and aging of Siberian biomass burning emissions in a large aerosol chamber, Atmospheric Environment, 185, 15-28, https://doi.org/10.1016/j.atmosenv.2018.04.033, 2018b.
Kaufman, Y., Ichoku, C., Giglio, L., Korontzi, S., Chu, D., Hao, W., Li, R.-R., and Justice, C.: Fire and smoke observed from the Earth Observing System MODIS instrument--products, validation, and operational use, International Journal of Remote Sensing, 24, 1765-1781, 2003.

Klimont, Z., Kupiainen, K., Heyes, C., Purohit, P., Cofala, J., Rafaj, P., Borken-Kleefeld, J., and Schöpp, W.: Global anthropogenic emissions of particulate matter including black carbon, Atmospheric Chemistry and Physics Discussions, 17, 8681-8723, 2017.
Kozlov, V. S., Panchenko, M. V., Shmargunov, V. P., Chernov, D. G., Yausheva, E. P., Pol'kin, V. V., and Terpugova, S. A.: Long-term investigations of the spatiotemporal variability of black carbon and aerosol concentrations in the troposphere of West Siberia and Russian Subarctic, Химия в интересах устойчивого развития, 24, 423-440, 2016.
Long, C. M., Nascarella, M. A., and Valberg, P. A.: Carbon black vs. black carbon and other airborne materials containing elemental carbon: Physical and chemical distinctions, Environmental Pollution, 181, 271-286, 2013.
Manousakas, M., Popovicheva, O., Evangeliou, N., Diapouli, E., Sitnikov, N., Shonija, N., and Eleftheriadis, K.: Aerosol carbonaceous, elemental and ionic composition variability and origin at the Siberian High Arctic, Cape Baranova, Tellus B: Chemical and Physical Meteorology, 72, 1-14, 2020.
Paris, J.-D., Stohl, A., Nédélec, P., Arshinov, M. Y., Panchenko, M., Shmargunov, V., Law, K. S., Belan, B., and Ciais, P.: Wildfire smoke in the Siberian Arctic in summer: source characterization and plume evolution from airborne measurements, Atmospheric Chemistry and Physics, 9, 9315-9327, 2009.
Pisso, I., Sollum, E., Grythe, H., Kristiansen, N. I., Cassiani, M., Eckhardt, S., Arnold, D., Morton, D., Thompson, R. L., and Groot Zwaaftink, C. D.: The Lagrangian particle dispersion model FLEXPART version 10.4, Geoscientific Model Development, 12, 4955-4997, 2019.
Popovicheva, O., Chichaeva, M., Kobelev, V., Sinitskiy, A., and Hansen, A.: Black Carbon in urban emissions on the Polar Circle, 26th International Symposium on Atmos. Ocean Optics, Proc. SPIE, 11560J,
Popovicheva, O., Timofeev, M., Persiantseva, N., Jefferson, M. A., Johnson, M., Rogak, S. N., and Baldelli, A.: Microstructure and chemical composition of particles from small-scale gas flaring, Aerosol and Air Quality Research, 19, 2205-2221, 2019a.
Popovicheva, O., Diapouli, E., Makshtas, A., Shonija, N., Manousakas, M., Saraga, D., Uttal, T., and Eleftheriadis, K.: East Siberian Arctic background and black carbon polluted aerosols at HMO Tiksi, Science of the Total Environment, 655, 924-938, 2019b.
Popovicheva, O. B., Evangeliou, N., Eleftheriadis, K., Kalogridis, A. C., Sitnikov, N., Eckhardt, S., and Stohl, A.: Black Carbon Sources Constrained by Observations in the Russian High Arctic, Environmental Science & Technology, 51, 3871-3879, 10.1021/acs.est.6b05832, 2017.
Qi, L. and Wang, S.: Sources of black carbon in the atmosphere and in snow in the Arctic, Science of The Total Environment, 691, 442-454, 2019.
Quinn, P. K., Bates, T. S., Baum, E., Doubleday, N., Fiore, A. M., Flanner, M., Fridlind, A., Garrett, T. J., Koch, D., Menon, S., Shindell, D., Stohl, A., and Warren, S. G.: Short-lived pollutants in the Arctic: their climate impact and possible mitigation strategies, Atmos. Chem. Phys., 8, 1723-1735, 10.5194/acp-8-1723-2008, 2008.
Randerson, J., Chen, Y., Van Der Werf, G., Rogers, B., and Morton, D.: Global burned area and biomass burning emissions from small fires, Journal of Geophysical Research: Biogeosciences, 117, 2012.
Ren, L., Yang, Y., Wang, H., Zhang, R., Wang, P., and Liao, H.: Source attribution of Arctic black carbon and sulfate aerosols and associated Arctic surface warming during 1980–2018, Atmospheric Chemistry and Physics, 20, 9067-9085, 2020.
Romshoo, B., Müller, T., Pfeifer, S., Saturno, J., Nowak, A., Ciupek, K., Quincey, P., and Wiedensohler, A.: Optical properties of coated black carbon aggregates: numerical simulations, radiative forcing estimates, and size-resolved parameterization scheme, Atmos. Chem. Phys., 21, 12989-13010, 10.5194/acp-21-12989-2021, 2021.
Saleh, R., Hennigan, C., McMeeking, G., Chuang, W., Robinson, E., Coe, H., Donahue, N., and Robinson, A.: Absorptivity of brown carbon in fresh and photo-chemically aged biomass-burning emissions, Atmospheric Chemistry and Physics, 13, 7683-7693, 2013.

Sandradewi, J., Prévôt, A. S., Szidat, S., Perron, N., Alfarra, M. R., Lanz, V. A., Weingartner, E., and Baltensperger, U.: Using aerosol light absorption measurements for the quantitative determination of wood burning and traffic emission contributions to particulate matter, Environmental science & technology, 42, 3316-3323, 2008.
Schacht, J., Heinold, B., Quaas, J., Backman, J., Cherian, R., Ehrlich, A., Herber, A., Huang, W. T. K., Kondo, Y., Massling, A., Sinha, P. R., Weinzierl, B., Zanatta, M., and Tegen, I.: The importance of the representation of air pollution emissions for the modeled distribution and radiative effects of black carbon in the Arctic, Atmos. Chem. Phys., 19, 11159-11183, 10.5194/acp-19-11159-2019, 2019.
Sharma, S., Lavoué, D., Cachier, H., Barrie, L., and Gong, S.: Long-term trends of the black carbon concentrations in the Canadian Arctic, Journal of Geophysical Research: Atmospheres, 109, 2004.
Stathopoulos, V., Evangeliou, N., Stohl, A., Vratolis, S., Matsoukas, C., and Eleftheriadis, K.: Large circulation patterns strongly modulate long term variability of Arctic black carbon levels and areas of origin, Geophysical Research Letters, e2021GL092876, 2021.
Stohl, A.: Characteristics of atmospheric transport into the Arctic troposphere, Journal of Geophysical Research: Atmospheres, 111, n/a-n/a, 10.1029/2005JD006888, 2006.
Stohl, A., Forster, C., Frank, A., Seibert, P., and Wotawa, G.: Technical note: The Lagrangian particle dispersion model FLEXPART version 6.2, Atmos. Chem. Phys., 5, 2461-2474, 10.5194/acp-5-2461-2005, 2005.
Stohl, A., Klimont, Z., Eckhardt, S., Kupiainen, K., Shevchenko, V. P., Kopeikin, V. M., and Novigatsky, A. N.: Black carbon in the Arctic: the underestimated role of gas flaring and residential combustion emissions, Atmos. Chem. Phys., 13, 8833-8855, 10.5194/acp-13-8833-2013, 2013.
Stohl, A., Andrews, E., Burkhart, J., Forster, C., Herber, A., Hoch, S., Kowal, D., Lunder, C., Mefford, T., and Ogren, J.: Pan-Arctic enhancements of light absorbing aerosol concentrations due to North American boreal forest fires during summer 2004, Journal of Geophysical Research: Atmospheres, 111, 2006.
Stohl, A., Berg, T., Burkhart, J., Fjæraa, A., Forster, C., Herber, A., Hov, Ø., Lunder, C., McMillan, W., and Oltmans, S.: Arctic smoke–record high air pollution levels in the European Arctic due to agricultural fires in Eastern Europe in spring 2006, Atmospheric Chemistry and Physics, 7, 511-534, 2007.
Stone, R. S., Sharma, S., Herber, A., Eleftheriadis, K., and Nelson, D. W.: A characterization of Arctic aerosols on the basis of aerosol optical depth and black carbon measurements, Elem Sci Anth, 2, 2014.
Treffeisen, R., Turnved, P., StrÖm, J., Herber, A., Bareiss, J., Helbig, A., Stone, R. S., Hoyningen-Huene, W., Krejci, R., Stohl, A., and Neuber, R.: Arctic smoke ? aerosol characteristics during a record air pollution event in the European Arctic and its radiative impact, Atmospheric Chemistry and Physics Discussions, 7, 2275-2324, 2007.
Tunved, P., Ström, J., and Krejci, R.: Arctic aerosol life cycle: linking aerosol size distributions observed between 2000 and 2010 with air mass transport and precipitation at Zeppelin station, Ny-Å lesund, Svalbard, Atmospheric Chemistry & Physics, 13, 3643-3660, 2013.
Vinogradova, A.: Anthropogenic Black Carbon emissions to the atmosphere: surface distribution through Russian territory, Atmospheric and Oceanic Optics, 28, 158-164, 2015.
Virkkula, A.: Modeled source apportionment of black carbon particles coated with a light-scattering shell, Atmospheric Measurement Techniques, 14, 3707-3719, 2021.
Voronova, O., Zima, A., Kladov, V., and Cherepanova, E.: Anomalous Wildfires in Siberia in Summer 2019, Izvestiya, Atmospheric and Oceanic Physics, 56, 1042-1052, 2020.
Wang, Q., Jacob, D. J., Fisher, J. A., Mao, J., Leibensperger, E. M., Carouge, C. C., Le Sager, P., Kondo, Y., Jimenez, J. L., Cubison, M. J., and Doherty, S. J.: Sources of carbonaceous aerosols and deposited black carbon in the Arctic in winter-spring: implications for radiative forcing, Atmos. Chem. Phys., 11, 12453-12473, 10.5194/acp-11-12453-2011, 2011.

Warneke, C., Froyd, K., Brioude, J., Bahreini, R., Brock, C., Cozic, J., De Gouw, J., Fahey, D., Ferrare, R., and Holloway, J.: An important contribution to springtime Arctic aerosol from biomass burning in Russia, Geophysical Research Letters, 37, 2010.
Werf, G. R., Randerson, J. T., Giglio, L., Leeuwen, T. T. v., Chen, Y., Rogers, B. M., Mu, M., Van Marle, M. J., Morton, D. C., and Collatz, G. J.: Global fire emissions estimates during 1997–2016, Earth System Science Data, 9, 697-720, 2017.
Winiger, P., Andersson, A., Eckhardt, S., Stohl, A., and Gustafsson, Ö.: The sources of atmospheric black carbon at a European gateway to the Arctic, Nature communications, 7, 1-8, 2016.
Winiger, P., Andersson, A., Eckhardt, S., Stohl, A., Semiletov, I. P., Dudarev, O. V., Charkin, A., Shakhova, N., Klimont, Z., Heyes, C., and Gustafsson, Ö.: Siberian Arctic black carbon sources constrained by model and observation, Proceedings of the National Academy of Sciences, 114, E1054-E1061, 10.1073/pnas.1613401114, 2017.
Wooster, M. J., Roberts, G., Perry, G., and Kaufman, Y.: Retrieval of biomass combustion rates and totals from fire radiative power observations: FRP derivation and calibration relationships between biomass consumption and fire radiative energy release, Journal of Geophysical Research: Atmospheres, 110, 2005.
Yun, Y., Penner, J. E., and Popovicheva, O.: The effects of hygroscopicity on ice nucleation of fossil fuel combustion aerosols in mixed-phase clouds, Atmos. Chem. Phys., 13, 4339-4348, 10.5194/acp-13-4339-2013, 2013.
Zhu, C., Kanaya, Y., Takigawa, M., Ikeda, K., Tanimoto, H., Taketani, F., Miyakawa, T., Kobayashi, H., and Pisso, I.: FLEXPART v10. 1 simulation of source contributions to Arctic black carbon, Atmospheric Chemistry and Physics, 20, 1641-1656, 2020.
Zotter, P., Herich, H., Gysel, M., El-Haddad, I., Zhang, Y., Močnik, G., Hüglin, C., Baltensperger, U., Szidat, S., and Prévôt, A. S.: Evaluation of the absorption Ångström exponents for traffic and wood burning in the Aethalometer-based source apportionment using radiocarbon measurements of ambient aerosol, Atmospheric Chemistry and Physics, 17, 4229-4249, 2017.

FIGURE LEGENDS

Figure 1. Top left map shows the location of the newly established "Island Bely" aerosol station in contrast to other Arctic stations (Zeppelin, Alert, Barrow, Summit, Tiksi, and Cape Baranova). Bottom left map shows a zoomed version of the location of the Bely Island in the Kara Sea, where the new station was developed (73°20'7.57"N, 70°4'49.05"E). The map on the right shows the "Island Bely" aerosol station in combination with the European part of Russia and Western Siberia and the Yamalo-Nenets Autonomic Okrug (YNAO). Flares of oil and gas fields are shown for 2019 year in brown triangles (adopted from https://skytruth.org/).

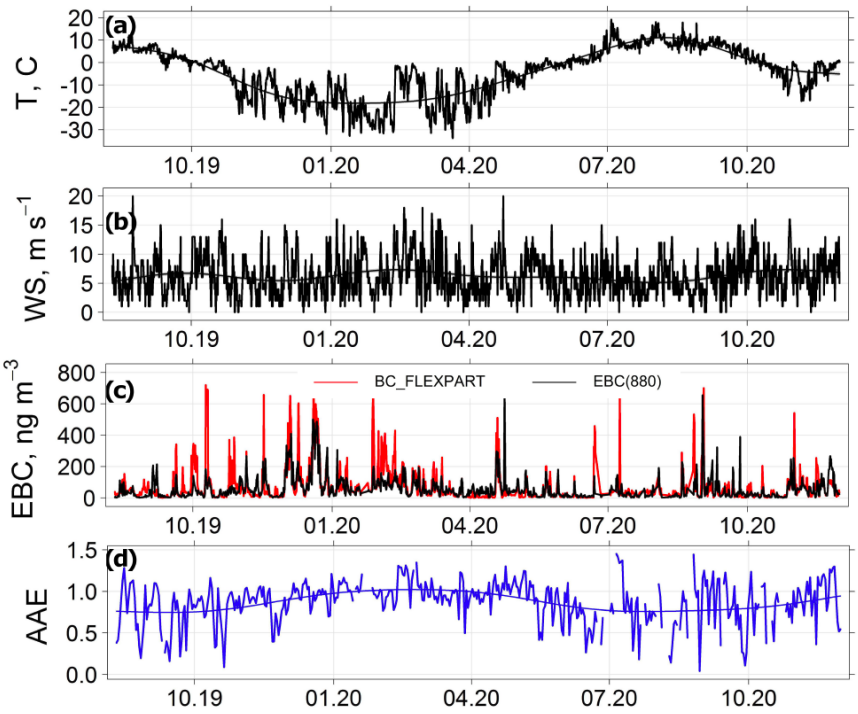

Figure 2. Meteorological conditions with respect to (a) mean temperature and (b) wind speed (data were smoothed to show long-term variations), (c) time-series of 24-h median EBC (black) and model BC using ECLIPSEv6 - CAMS emissions (red), and (d) 24-h average Absorption Ångström Exponent (AAE) measured at "Island Bely" station from 10 August 2019 to 30 November 2020 (date format in mm.yy).

Deleted: (c)

Deleted: simulated

Deleted: absorption

Deleted: exponent

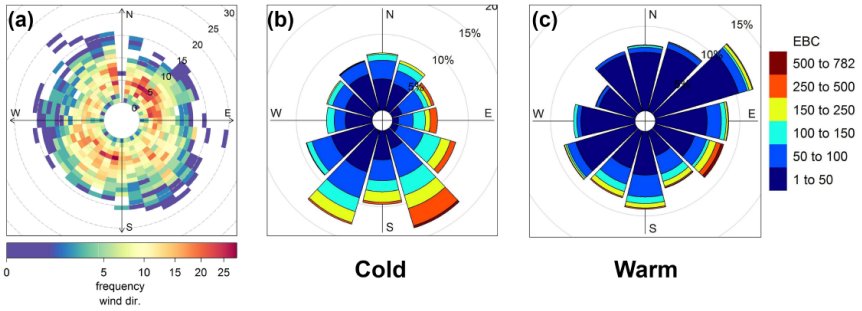

Figure 3. (a) Polar frequency plots of wind speed and direction. Each cell gives the total number of hours the wind was originating from a certain wind direction. The dashed circular grey lines show the wind speed (in m s^{-1}). Rose diagrams showing 3h EBC concentrations during the cold (b) and warm (c) periods.

Deleted: ing

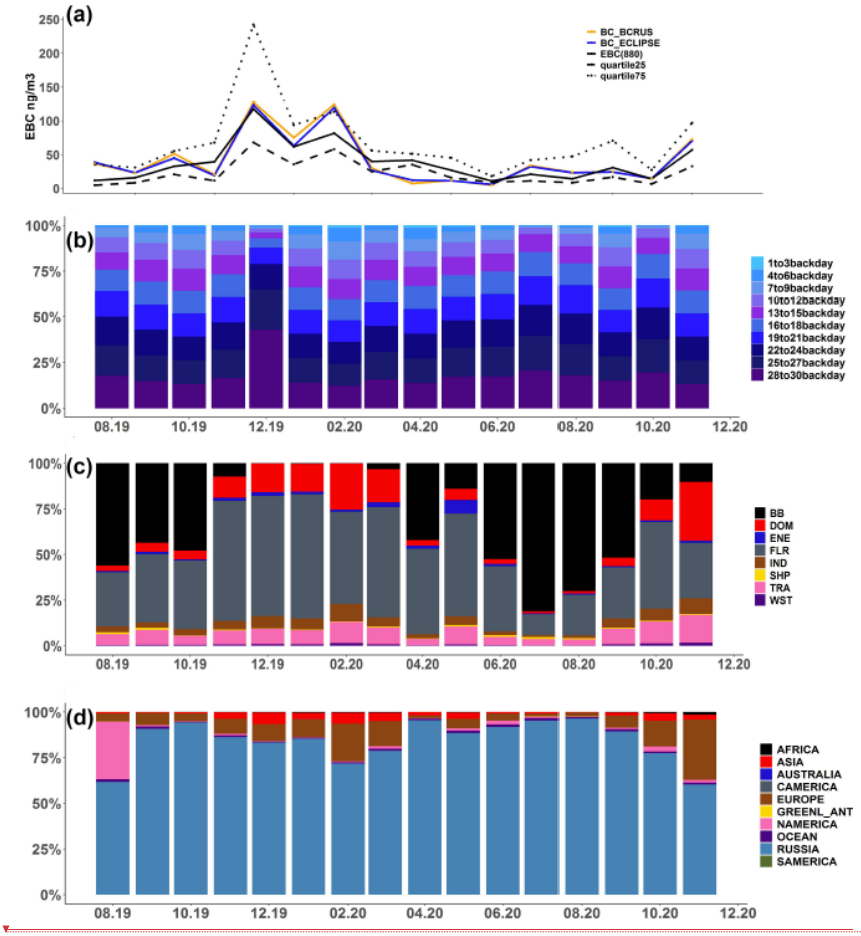

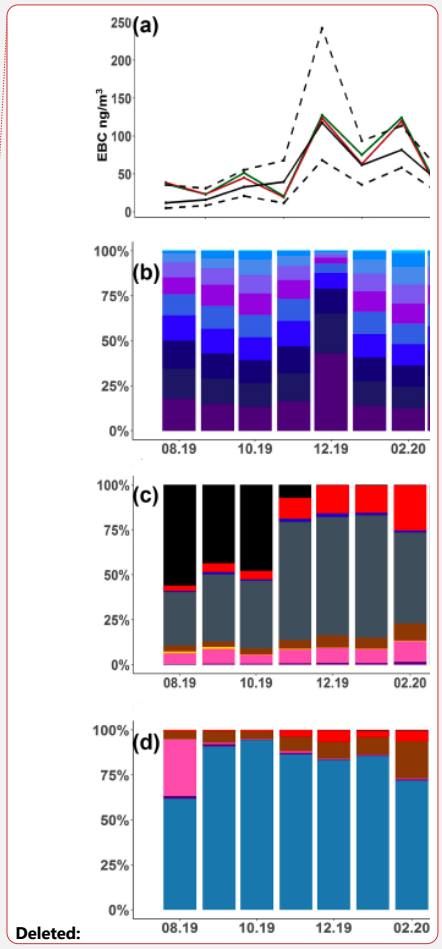

Deleted:

Figure 4. (a) Monthly climatology of EBC at the "Island Bely" station depicting medians, 25th and 75th percentiles (dashed lines). Near-surface monthly median BC concentrations simulated with FLEXPART coupled to ECLIPSEv6-CAMS (steel blue) and ECLIPSEv6-BCRUS-CAMS (red) emissions are also shown. (b) Age spectrum of modelled BC from all possible sources showing the contribution of emissions from each day back in time to the surface concentration of BC. (c) Contribution from different emission source types to surface BC concentrations. The emission sources of biomass burning (BB) adopted from GFEDv4.1, and residential and commercial (DOM), power plants, energy conversion, and extraction (ENE), gas flaring (FLR), industrial combustion and processing (IND), shipping (SHP), and transportation (TRA) adopted from ECLIPSEv6 were considered. (d) Continental spectrum showing the contribution from each continent or region to surface BC concentrations. 10 regions were considered namely, Africa, Asia, Australia, Central America, Europe, Greenland/Antarctica, North America, World Ocean, Russia, and South America (see Supplementary Figure S 3).

Deleted: mass

Deleted: with

Deleted:

Deleted: inventories

Deleted: of

Deleted: of BC

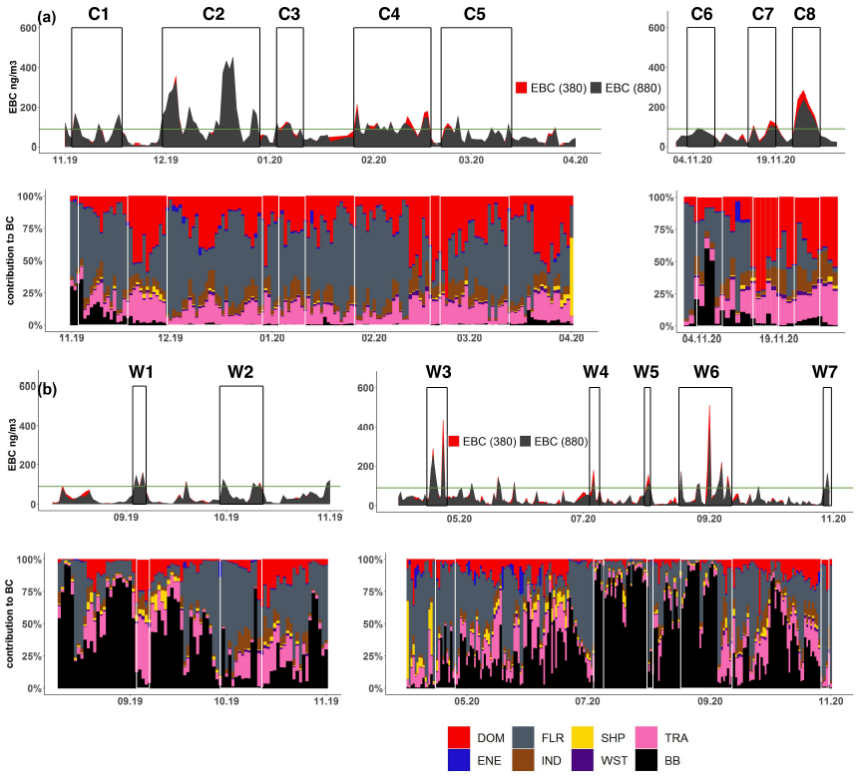

Figure 5. 24-h median EBC concentrations measured at 880 nm (black) and 370 nm (red), and source contributions to surface BC from anthropogenic (DOM, ENE, FLR, IND, SHP, WST, TRA) and BB sources for (a) the cold and (b) the warm period. Pollution episodes were composed from the periodically repeated events of high EBC concentration. The green straight line indicates the pollution level of the 80th percentile.

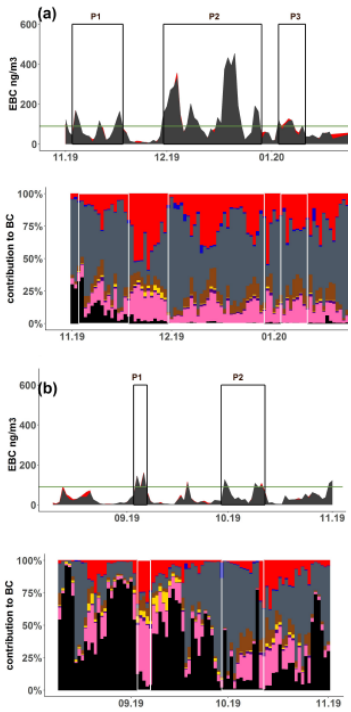

Deleted:

Deleted: our

Deleted: (P1-P8)

Deleted: are

Deleted: est

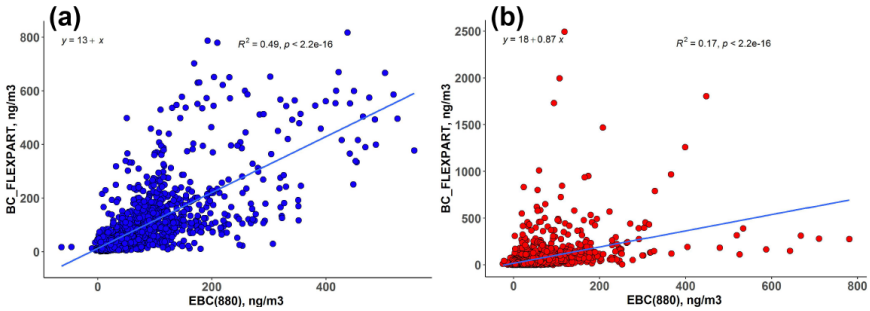

Figure 6. Scatter-plots of 3-h median measured EBC (880) against modelled BC from FLEXPART for the (a) cold and (b) warm period. Solid line is the linear regression fit of the comparison between modelled and observed values.

Deleted: and

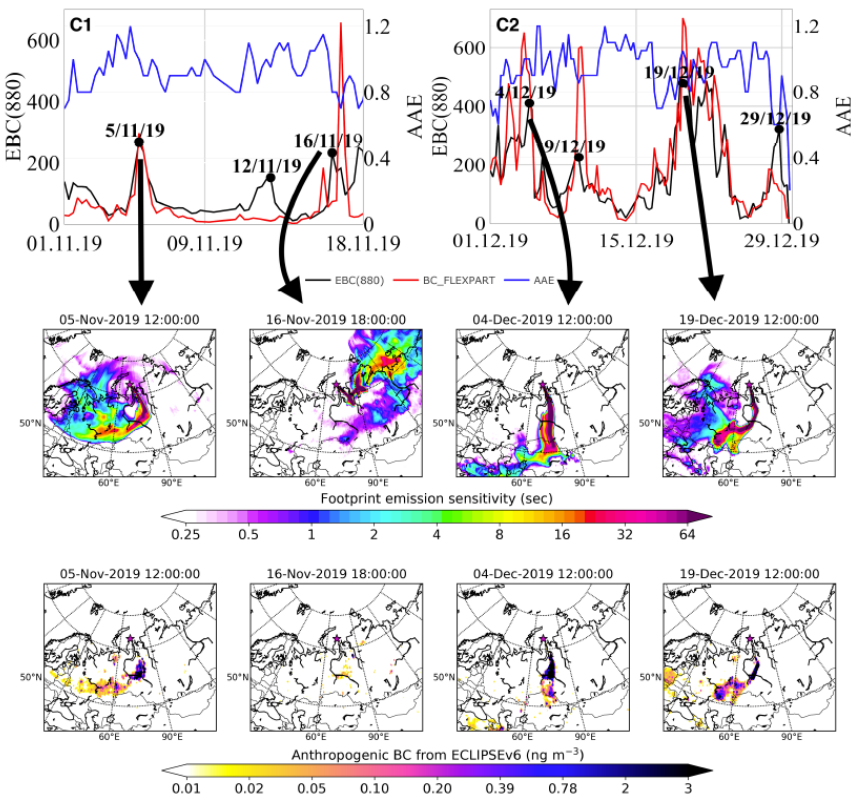

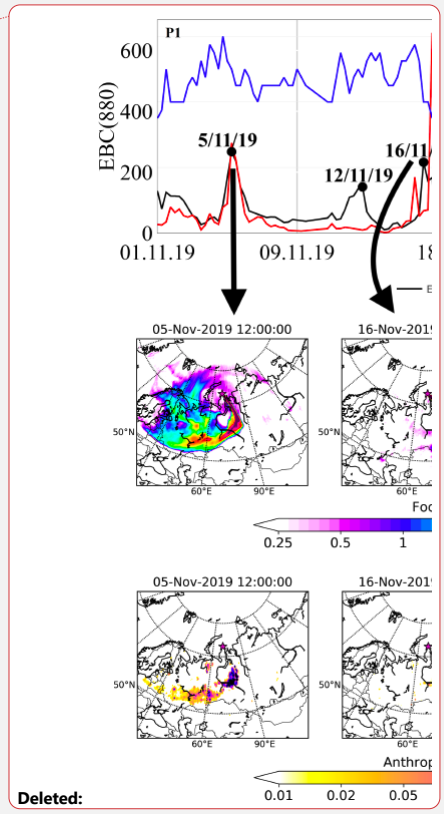

Deleted:

Figure 7. Examples of pollution episodes C1 and C2 observed in the cold period (see **Figure 5**a), where FLR contribution prevails. 6-h median EBC (880) (black line), BC simulated with FLEXPART (red line), AAE (blue line) (upper row). Footprint emissions sensitivities in seconds showing the largest probability of emission origin (middle row). Spatial distribution of anthropogenic contribution (in ng/m3) to surface BC at the "Island Bely" station (bottom row).

Deleted: P1

Deleted: P2

Deleted: **Figure 5**

Deleted: ourly

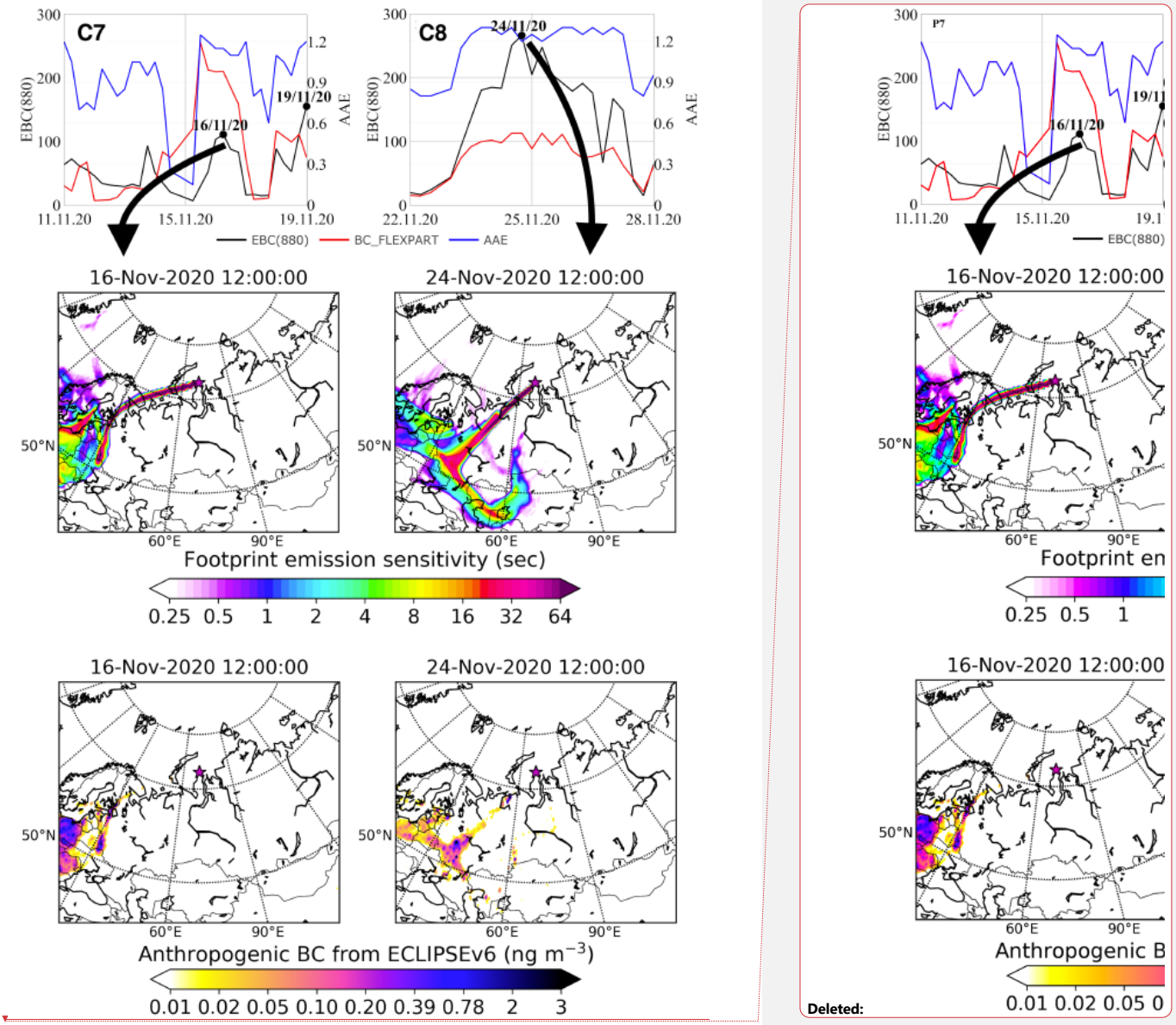

Figure 8. Examples of pollution episodes C7 and C8 observed in the cold period (see Figure 5a), where DOM and TRA contribution prevails. Timeseries of measured EBC, modelled BC and AAE (upper row), footprint emissions sensitivities (middle row) and anthropogenic contribution to surface BC (bottom row) are shown.

Deleted:

Deleted: P7

Deleted: P8

Deleted: Figure 5

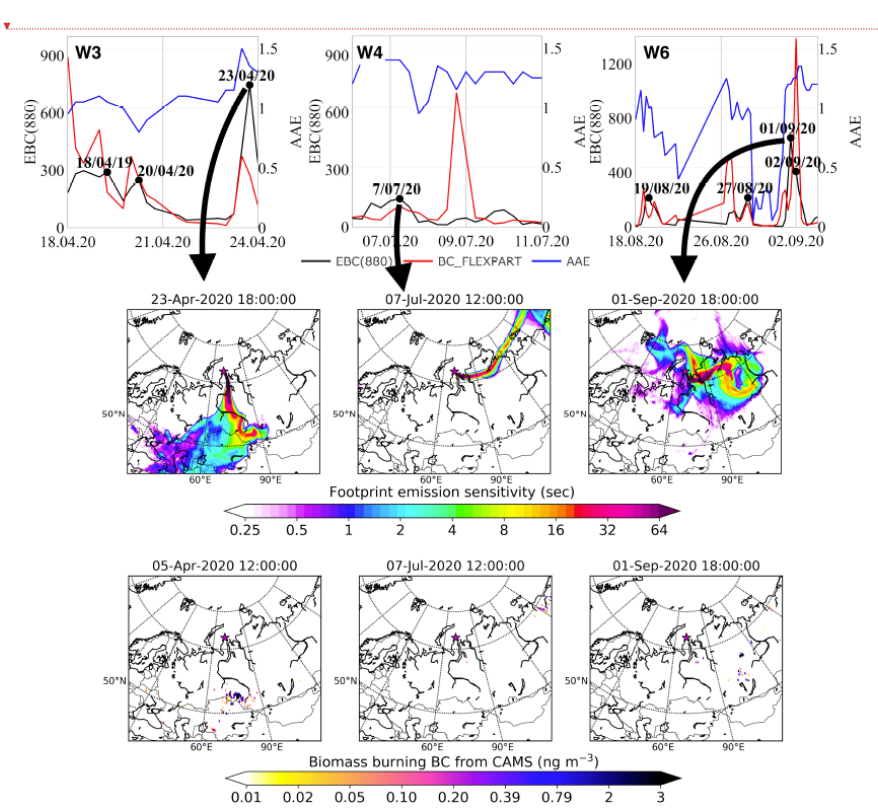

Figure 9. Examples of pollution episodes W3, W4 and W6 in the warm period (see Figure 5b), where BB contribution prevails. The figure has been arranged similar to Figure 7 (timeseries of measured EBC, modelled BC and AAE, footprint emissions sensitivities and BB contribution to surface BC).

Deleted:

Deleted: P

Deleted: P

Deleted: P

Deleted: Figure 5

Deleted: Figure 7